Wingman-based Estimation and Guidance for a Sensorless PN-Guided Pursuer

Fonod, R.; Shima, Tal

DOI
10.1109/TAES.2019.2935642

Publication date
2019

Document Version
Accepted author manuscript

Published in
IEEE Transactions on Aerospace and Electronic Systems

Citation (APA)
Fonod, R., & Shima, T. (2019). Wingman-based Estimation and Guidance for a Sensorless PN-Guided Pursuer. *IEEE Transactions on Aerospace and Electronic Systems*, *56*(3), 1754-1766. Article 8801859. Advance online publication. https://doi.org/10.1109/TAES.2019.2935642

This article has been accepted for publication in a future issue of this journal, but has not been fully edited. Content may change prior to final publication. Citation information: DOI 10.1109/TAES.2019.2935642, IEEE Transactions on Aerospace and Electronic Systems

Wingman-based Estimation and Guidance for a Sensorless PN-Guided Pursuer

Robert Fonod, *Member, IEEE* and Tal Shima, *Senior Member, IEEE*

***Abstract*—A novel wingman-based estimation and guidance concept is proposed for a sensorless pursuer. The pursuer is guided towards a maneuvering aerial target using proportional navigation (PN) guidance law. The wingman is assumed to acquire bearings-only measurements of the target and to accurately track the wingman-pursuer relative position. The pursuer-target relative states, needed for the pursuer guidance law implementation, are estimated from the available data to the wingman. The proposed state estimator is implemented using extended Kalman filter equations and transformed wingman's measurements into the moving pursuer frame. Analytical observability analysis of the proposed wingman-based measuring concept suggests an optimal wingman trajectory in terms of the wingman-pursuer relative geometry. The resulting wingman trajectory ensures maximum observability of the pursuer–target line-of-sight (LOS) angle, which is a crucial parameter needed for the PN guidance law implementation. The resulting trajectory can be directly related to the well-known LOS guidance concept. Monte Carlo simulation results validate the analytical findings and demonstrate the potential of the proposed concept.**

***Index Terms*—Observability, PN guidance law, state estimation, optimal trajectory, extended Kalman filter.**

I. Introduction

MODERN air defense systems, such as aircraft defending missiles or anti-ballistic missiles, are equipped with highly sophisticated sensors and on-board computers. As payloads, these equipment place significant requirements on the missile's weight, power, cost, and volume. In most cases, the re-usability of these valued equipment is not possible due to the fact that they cease to exist after the end of the engagement.

In this paper, we propose a new estimation and guidance concept for a pursuing missile which does not require any target-tracking sensors nor a powerful on-board guidance computer. This concept relies on the availability of a single wingman vehicle, equipped with suitable sensors and on-board computing power. The wingman only guides the pursuing missile to the aerial target, but is not actively engaged in the interception. The missile's guidance law is computed in the wingman's on-board computer and is transmitted to the missile for execution. This enables to design a defender missile with reduced complexity, weight, cost, and footprint. Moreover, precious wingman components, such as sensor suites and on-board computers, can be saved and reused for future engagements. Thanks to the wingman's re-usability, implementation of more advanced and computationally demanding guidance and estimation algorithm may be possible, while maintaining or even minimizing the overall engagement costs.

Practical guidance laws require estimation and filtering of various missile-target states. Observability of unmeasured states represents a fundamental issue in state estimation. Different guidance laws pose different requirements on the accuracy of the relative state estimates. Therefore, in this paper, we will focus only on one guidance law for the missile, namely the proportional navigation (PN) guidance law. Many air/surface-to-air/surface missile-target engagements, as well as space applications (including rendezvous), employ some version of PN guidance law. This guidance law can provide satisfactory interception against a non-maneuvering or weakly maneuvering targets. Moreover, the PN guidance law is also popular because of its robustness, ease of implementation, and simplicity [1]. Under certain conditions and simplifying assumptions, the PN guidance law is an optimal guidance strategy minimizing the terminal miss distance [2].

Target-tracking and observability-enhancing guidance systems in homing missiles that use bearings-only measurements have been comprehensively studied in the past [3]–[7]. However, to the best of the authors knowledge, no such study has been done for a PN-guided sensorless missile aided by a wingman vehicle having bearings only measurements. For this reason, the main contributions of this paper are as follows. First, a wingman-based target tracking estimator is developed to estimate the missile–target kinematic variables which are needed for a proper implementation of the sensorless missile's PN guidance law. Second, a novel observability metrics for the missile-target range and line-of-sight (LOS) angle are derived analytically. This is achieved by transforming the wingman's bearings-only measurements into the missile frame and subsequently computing, using analytical linearization, the variances of the resulting pseudo-measurements. Insights gained from these metrics suggest that the wingman trajectory, which aims at maximizing the PN-guided missile's homing performance, should be designed such that the wingman maintains its position on the extended missile-target LOS line.

The remainder of this paper is organized as follows. The next section presents the mathematical models and assumptions of the wingman-missile-target engagement. The target tracking estimator is presented in Sec. III, followed by the analytical observability metrics derivation in Sec. IV. Trajectory implications of the wingman are discussed in Sec. V. Simulation results are presented in Sec. VI, followed by concluding remarks.

Notations: In this paper, bold italic face denotes vectors and matrices; $(\cdot)^T$ stands for transposition; $\boldsymbol{I}$ represents an identity matrix with appropriate dimensions; $\mathbb{R}^n$ represents the

R. Fonod is with the Faculty of Aerospace Engineering, Delft University of Technology, Delft 2629 HS, The Netherlands (e-mail: r.fonod@tudelft.nl).
T. Shima is with the Department of Aerospace Engineering, Technion - Israel Institute of Technology, Haifa 3200003, Israel (e-mail: tal.shima@technion.ac.il).

This article has been accepted for publication in a future issue of this journal, but has not been fully edited. Content may change prior to final publication. Citation information: DOI 10.1109/TAES.2019.2935642, IEEE Transactions on Aerospace and Electronic Systems

set of n dimensional real vectors; $\mathbb{N}$ the set of natural numbers (including $\{0\}$); and $\mathcal{N}(\boldsymbol{\mu}, \boldsymbol{\Sigma})$ denotes, in general, the density function of a non-degenerate multivariate normal distribution with a mean vector $\boldsymbol{\mu}$ and covariance matrix $\boldsymbol{\Sigma}$.

II. Engagement

This section presents the kinematics, dynamics, and timeline of the considered engagement. The wingman's measurement model is introduced alongside with the missile's guidance law. The underlying assumptions are also discussed.

A. Kinematics and Dynamics

Consider a planar engagement scenario shown in Fig. 1, where a sensorless homing missile M pursues a maneuvering aerial target T with a help of a wingman vehicle W. For brevity, in the rest of the paper, the homing missile is referred to as missile or pursuer, the wingman vehicle as wingman, and the aerial target as target.

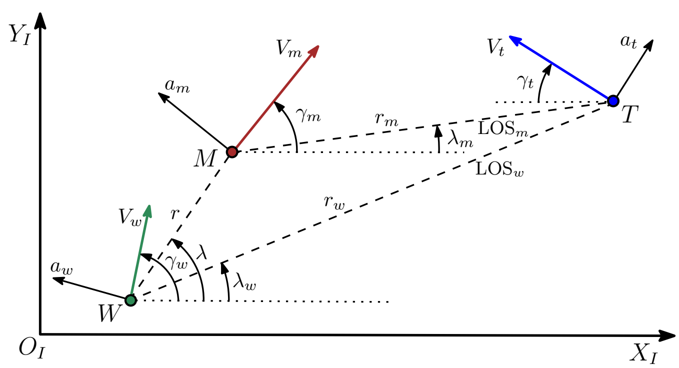

Fig. 1. Planar engagement geometry.

In Fig. 1, the Cartesian inertial reference frame is denoted by X_I–O_I–Y_I. The speed, normal acceleration, and flight-path angle are given by V, a, and γ; subscript m, w, and t denotes the missile, wingman, and target, respectively. The range between the wingman-missile (W–M), missile-target (M–T), and wingman-target (W–T) are denoted as r, r_m, and r_w, respectively. The angle between the missile-to-target LOS (LOS_m) and the X_I axis is denoted as λ_m. Similarly, the angle between LOS_w and the X_I axis is denoted as λ_w, whereas the angle between the missile-to-wingman LOS and the X_I axis is denoted as λ. All angles are measured in a counter-clockwise direction from the positive X_I axis.

All three vehicles are assumed to be skid-to-turn roll-stabilized. Additionally, assuming M, W, and T being point-masses and neglecting the effects of gravity, the M–T and the W–T engagement kinematics can be expressed in polar coordinates (r_i, λ_i), $i \in \{m, w\}$, as follows[1]

$$\dot{r}_i = -V_i \cos(\gamma_i - \lambda_i) - V_t \cos(\gamma_t + \lambda_i) \triangleq V_{r,i}, \tag{1a}$$

$$\dot{\lambda}_i = \frac{-V_i \sin(\gamma_i - \lambda_i) + V_t \sin(\gamma_t + \lambda_i)}{r_i} \triangleq \frac{V_{\lambda,i}}{r_i}, \tag{1b}$$

[1]For sake of clarity, the notation of time-dependency (t) of some variables is omitted whenever the context is clear. Subscript "t" always refers to the target vehicle.

where $V_{r,i}$ is the relative velocity along, and $V_{\lambda,i}$ normal, to LOS_i. It is assumed that $r_i(0) > 0$ and $|\lambda_i(0)| \leq \pi/2$.

During the endgame, all vehicles are assumed to fly at constant speeds and to perform lateral maneuvers only, therefore

$$\dot{\gamma}_v = a_v / V_v, \tag{2a}$$

$$\dot{V}_v = 0, \tag{2b}$$

where $v \in \{m, w, t\}$. In addition, first-order maneuver dynamics is considered for all vehicles, i.e.,

$$\dot{a}_v = (u_v - a_v)/\tau_v. \tag{3}$$

In (3), u_v is the vehicle's piece-wise continuous acceleration command and $\tau_v > 0$ is the time constant of the vehicle's dynamics. We also assume that all vehicles have maneuverability limitations defined as

$$|u_v| \leq a_v^{max}, \tag{4}$$

where $a_v^{max} > 0$ is the vehicle's maximal lateral acceleration.

B. Timeline

We denote the running time as t. The engagement starts at $t = t_0 \triangleq 0$ with $\dot{r}_m(t_0) < 0$. The endgame terminates at $t = t_f$, where t_f is the M–T interception time defined as

$$t_f \triangleq \arg \inf_{t>0} \left(r_m(t) \dot{r}_m(t) = 0 \right). \tag{5}$$

The interception time t_f allows to define the non-negative missile-to-target time-to-go t_{go} as

$$t_{go} \triangleq \begin{cases} t_f - t, & t \leq t_f \\ 0, & t > t_f \end{cases} \tag{6}$$

At $t = t_f$, the M–T range, $r_m(t_f)$, is minimal and will be referred to as "miss distance" or compactly as "miss".

Since the exact value of t_f is hard to compute, a common approximation of t_{go} is

$$t_{go} \approx -r_m / V_{r,m}, \qquad V_{r,m} < 0, \tag{7}$$

where $V_{r,m}$ is given in (1a). Note, (7) is valid provided the engagement is very close to the collision course. For larger heading errors, more accurate time-to-go approximations should be considered, see for instance [8], [9] and references therein.

C. Wingman's Measurement Model

For the wingman–missile team, we assume that only the wingman is equipped with sensors that are able to track the target motion. Particularly, we assume that the wingman is equipped with an IR sensor, measuring the wingman–target LOS angle λ_w. These measurements, z_k, $k \in \mathbb{N}$, are assumed to be acquired at discrete-time instances $t = t_k \triangleq kT$, where $T_s > 0$ is a fixed measurement sampling period. Additionally, the measurements are assumed to be contaminated by a zero-mean white Gaussian noise sequence, $v_{\lambda_w;k}$, $k \in \mathbb{N}$, having a time-invariant standard deviation $\sigma_{\lambda,w} > 0$. Based on the above assumptions, the physical measurement model of the wingman's sensor measurements is

$$z_k = \lambda_{w;k} + v_{\lambda_w;k}, \qquad v_{\lambda_w;k} \sim \mathcal{N}(0, \sigma^2_{\lambda,w}), \tag{8}$$

where $\lambda_{w;k}$ is the LOS angle λ_w at $t = t_k$, i.e., $\lambda_{w;k} \triangleq \lambda_w(t_k)$. Henceforth, the subscript k, separated by a semicolon if necessary, will denote the discrete-time t_k.

D. Missile's Guidance Law

Most of the guidance laws are implemented using the kinematics and dynamics variables. For the M–T engagement, these variables can be lumped into the following state vector

$$\boldsymbol{x}_m \triangleq \begin{bmatrix} r_m & \lambda_m & \gamma_t & a_t & V_t \end{bmatrix}^T. \tag{9}$$

The acceleration command u_m normal to the velocity vector of a PN-guided missile can be expressed using the state vector $\boldsymbol{x}_m$ and the known flight-related parameters of the missile (γ_m and V_m) as follows

$$u_m(\boldsymbol{x}_m) = N' \frac{V_{c,m}\dot{\lambda}_m}{\cos(\gamma_m - \lambda_m)}, \tag{10}$$

where N' is the effective navigation gain, normally having an integer value of 3, 4, or 5, and $V_{c,m}$ is the M–T closing velocity defined as $V_{c,m} \triangleq -V_{r,m}$. (Similarly, the W–T closing velocity is defined as $V_{c,w} \triangleq -V_{r,w}$.) Variables $\dot{\lambda}_m$ and $V_{r,m}$ are given in (1). The term $\cos(\gamma_m - \lambda_m)$ in the denominator of (10) accounts for the LOS-to-body frame transformation.

E. Assumptions

Figure 2 summarizes the missile-target engagement dynamics in a block diagram form. It also includes the role of the wingman and the information flow between the vehicles.

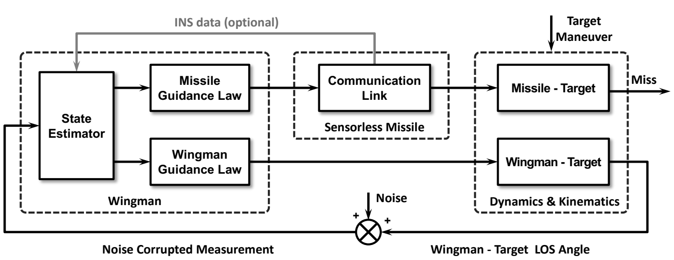

Fig. 2. Block diagram of the engagement dynamics.

In this paper, we adopt the following assumptions on the W–M kinematics, inertial sensors, and communications:

Assumption 1: The flight-related parameters, such as flight-path angle, lateral acceleration, and speed, of the wingman and the missile are available to the wingman to very high accuracy. This is a common assumption and can be accomplished by installing an inertial navigation system (INS) on both the wingman and the missile, and transmitting the missile's parameters (γ_m, a_m, and V_m) to the wingman.

Assumption 2: The wingman-missile relative distance (r and λ) is known accurately to the wingman (via some navigation system installed on the wingman).

Assumption 3: The missile's acceleration command u_m is computed in the wingman's on-board computer and is transmitted to the missile with zero lag. This minimizes the W–M communication overhead as, instead of all kinematic variables needed for the missile guidance law implementation, only u_m is transmitted to the missile.

Assumption 4: The missile and the wingman are launched simultaneously from the same location, i.e., $r(t_0) \approx 0$. To avoid wingman–target clash ($r_w = 0$), the wingman shall fly behind the missile at all times ($r_w > r_m$). This can be ensured by maintaining $V_{c,w}/V_{c,m} < 1$. This requirement naturally implies a set of feasible and infeasible W–M relative geometries, see Fig. 3 for illustration.

Assumption 5: The target acceleration $a_t(t)$ is viewed as a random process with unknown statistics.

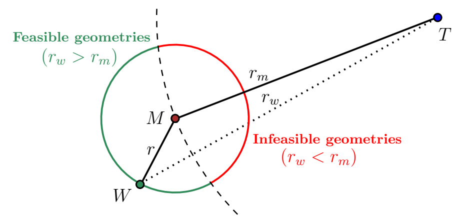

Fig. 3. Feasible vs. infeasible W–M geometries for a given r and r_m.

Remark 1. *Given u_m, accurate missile modeling, and accurate W–M relative position information (r, λ), the missile's flight-related parameters (γ_m, a_m, and V_m) can be directly estimated by the wingman. Consequently, the assumption on the availability of the INS for the missile, as discussed in Assumption 1, can be dropped.*

III. Estimator Design

The missile's state vector $\boldsymbol{x}_m$ needs to be estimated from the available data to the wingman. In this section, we will design a relatively simple target tracking estimator which can be run on the wingman.

A. Wingman's Measurements Expressed Using M–T Variables

Consider the engagement geometry depicted in Fig. 1 and the assumption that the relative position between W and M is know accurately to W. Let $\boldsymbol{\phi}$ denote the W–M relative position (r, λ). Then, using the trigonometric law of cosines, the LOS angle λ_w can be expressed as a function of $\boldsymbol{x}_m$ and $\boldsymbol{\phi}$, i.e.,

$$\lambda_w = h_w(\boldsymbol{x}_m, \boldsymbol{\phi}) \triangleq \lambda + s\left[\pi - \cos^{-1}\left(\frac{r_m^2 - r^2 - r_w^2}{2rr_w}\right)\right]. \tag{11}$$

Here, the W–T range, r_w, can be also expressed as a function of $\boldsymbol{x}_m$ and $\boldsymbol{\phi}$, that is

$$r_w = g_w(\boldsymbol{x}_m, \boldsymbol{\phi}) \triangleq \sqrt{r^2 + r_m^2 + 2rr_m\cos(\lambda_m - \lambda)}. \tag{12}$$

Note that in (11) and (12), the values of r_m, λ_m, r, and λ are substituted with corresponding entries from $\boldsymbol{x}_m$ and $\boldsymbol{\phi}$.

This article has been accepted for publication in a future issue of this journal, but has not been fully edited. Content may change prior to final publication. Citation information: DOI 10.1109/TAES.2019.2935642, IEEE Transactions on Aerospace and Electronic Systems

In (11), s stands for a sign function, which depends on the relative geometry between M and W, defined as

$$s \triangleq \begin{cases} 1, & \lambda_w > \lambda, \\ -1, & \lambda_w < \lambda, \\ 0, & \text{otherwise}. \end{cases} \tag{13}$$

Finally, the physical measurement model of the wingman (8) can be related to $\boldsymbol{x}_{m;k} \triangleq \boldsymbol{x}_m(t_k)$ and $\boldsymbol{\phi}_k \triangleq (r(t_k), \lambda(t_k))$ as follows

$$z_k = h_w\left(\boldsymbol{x}_{m;k}, \boldsymbol{\phi}_k\right) + v_{w;k}. \tag{14}$$

As will be shown next, the model of (14) allows the wingman to run an estimator on its own and to compute an estimate of $\boldsymbol{x}_{m;k}$ using $\boldsymbol{\phi}_k$ and $\boldsymbol{z}_{1:k} \triangleq \{z_1, z_2, \ldots, z_k\}$.

B. Target Maneuver Model Considerations

Since the target dynamics and target maneuver command u_t are rarely known in reality, an assumption must be established on the target maneuver model, i.e., on $a_t(t)$, in order to design a target tracking estimator.

In this paper, we adopt the Singer's exponentially correlated acceleration (ECA) model [10]. The ECA model is widely used for miscellaneous maneuvering target tracking problems. It suggests that maneuvers (turns, evasive maneuvers, and accelerations due to atmospheric disturbances), acting on constant-velocity moving targets, can be viewed as perturbations of the constant velocity trajectories and represented as random accelerations correlated in time.

To proceed, the ECA model assumes that the target acceleration $a_t(t)$ is a scalar stochastic process with the following, exponentially decaying, autocorrelation function

$$C_{a_t a_t}(\tau) \triangleq E\left[a_t(t+\tau)a_t(t)\right] = \sigma_t^2 e^{-\alpha|\tau|}, \tag{15}$$

where σ_t^2 is the instantaneous variance of the target acceleration and $\alpha > 0$ is the reciprocal of the time constant of the target acceleration autocorrelation [11]. For example, $\alpha \simeq 1/60$ for a lazy turn, $\alpha \simeq 1/20$ for an evasive maneuver, and $\alpha \simeq 1$ for atmospheric turbulence [10]. According to Singer [10], to provide satisfactory representation of the target's instantaneous maneuver characteristics, σ_t shall be chosen as follows:

$$\sigma_t = \Psi a_t^{max}, \tag{16}$$

where a_t^{max} is the target's maximal lateral acceleration and $\Psi = \sqrt{(1 - P_0 + 4P_{\max})/3}$. Here, $P_{\max}$ stands for the probability of the target accelerating at $\pm a_t^{max}$ and P_0 for the probability of the target not maneuvering. Since a_t^{max}, P_0, and P_{max} are rarely available in practice, Ψ is often used as the tuning parameter of the filter.

The process $a_t(t)$, characterized by (15), can be represented by a linear time-invariant system as follows [11]

$$\dot{a}_t(t) = -\alpha a_t(t) + w_t(t), \tag{17}$$

where $w_t(t)$ is a zero-mean, stationary, white Gaussian process, with the following autocorrelation function

$$C_{w_t w_t}(\tau) = 2\alpha\sigma_t^2\delta(\tau), \tag{18}$$

with $\delta(\tau)$ being the Dirac delta function.

Using (1), (2), and (17), the equations of motion (EOM) for the estimator design become

$$\dot{\boldsymbol{x}}_m = \boldsymbol{f}(\boldsymbol{x}_m) + \boldsymbol{G} w_t, \tag{19}$$

where

$$\boldsymbol{f}(\boldsymbol{x}_m) \triangleq \begin{bmatrix} V_{r,m} & V_{\lambda,m}/r_m & a_t/V_t & -\alpha a_t & 0 \end{bmatrix}^T \tag{20}$$

and $\boldsymbol{G} \triangleq \begin{bmatrix} 0 & 0 & 0 & 1 & 0 \end{bmatrix}^T$. The expressions for $V_{r,m}$ and $V_{\lambda,m}$ are given in (1).

Remark 2. *Other target maneuver models might be more appropriate in specific situations, see [12] for a good survey on target maneuvering models. For instance, if the target is assumed to perform optimal evasive maneuvers, which are known to have a "bang–bang" structure against a PN-guided missile [13], such maneuvers may be better described by a shaping filter [14], [15]. However, due to Assumption 5, the ECA model presented in this section is considered to be a good approximation to many random processes with unknown statistics.*

C. Discretization

The discrete-time version of (19) can be written as

$$\boldsymbol{x}_{m;k} = \boldsymbol{f}_{k-1}^d(\boldsymbol{x}_{m;k-1}) + \boldsymbol{w}_{t;k}, \tag{21}$$

where $\boldsymbol{f}_{k-1}^d(\cdot)$ is a vector function obtained by integrating (19) from t_{k-1} to t_k with initial condition $\boldsymbol{x}_m(t_{k-1}) = \boldsymbol{x}_{m;k-1}$ and setting $w_t(\tau)$ to zero for $\tau \in \langle t_{k-1}, t_k \rangle$. In (21), $\boldsymbol{w}_{t;k}$ represents a vector valued zero-mean white noise sequence which relates to the scalar continuous-time process $w_t(t)$ as follows

$$\boldsymbol{w}_{t;k} = \int_{t_{k-1}}^{t_k} e^{(t_k - \tau)\boldsymbol{F}_{k-1}} \boldsymbol{G}\, w_t(\tau) \mathrm{d}\tau, \tag{22}$$

where $\boldsymbol{F}_{k-1}$ is the Jacobian matrix associated with (20) and evaluated at $\boldsymbol{x}_{m;k-1}$, i.e.,

$$\begin{aligned} \boldsymbol{F}_{k-1} &\triangleq \left.\frac{\partial \boldsymbol{f}(\boldsymbol{x}_m)}{\partial \boldsymbol{x}_m}\right|_{\boldsymbol{x}_m = \boldsymbol{x}_{m;k-1}} \\ &= \left.\begin{bmatrix} 0 & F_{12} & F_{13} & 0 & F_{15} \\ F_{21} & F_{22} & F_{23} & 0 & F_{25} \\ 0 & 0 & 0 & 1/V_t & -a_t/V_t^2 \\ 0 & 0 & 0 & -\alpha & 0 \\ 0 & 0 & 0 & 0 & 0 \end{bmatrix}\right|_{\boldsymbol{x}_m = \boldsymbol{x}_{m;k-1}} \end{aligned} \tag{23}$$

where

$$\begin{aligned} F_{12} &= V_t \sin(\gamma_t + \lambda_m) - V_m \sin(\gamma_m - \lambda_m) \\ F_{13} &= V_t \sin(\gamma_t + \lambda_m) \\ F_{15} &= -\cos(\gamma_t + \lambda_m) \\ F_{21} &= \tfrac{1}{r_m^2}\left[V_m \sin(\gamma_m - \lambda_m) - V_t \sin(\gamma_t + \lambda_m)\right] \\ F_{22} &= \tfrac{1}{r_m}\left[V_m \cos(\gamma_m - \lambda_m) + V_t \cos(\gamma_t + \lambda_m)\right] \\ F_{23} &= \tfrac{1}{r_m} V_t \cos(\gamma_t + \lambda_m) \\ F_{25} &= \tfrac{1}{r_m} \sin(\gamma_t + \lambda_m) \end{aligned}$$

It is assumed that $\boldsymbol{F}_{k-1}$ is fixed during the time interval $(t_{k-1}, t_k\rangle$. With the zero-mean and white assumption on $w_t(t)$, it follows that $\boldsymbol{w}_{t;k}$ satisfies

$$E[\boldsymbol{w}_{t;k}] = \boldsymbol{0}, \qquad E[\boldsymbol{w}_{t;k}\boldsymbol{w}_{t;j}^T] = \boldsymbol{Q}_k\delta_{k,j}, \tag{24}$$

where $\delta_{k,j}$ is the Kronecker delta ($\delta_{k,j} = 1$ if $k = j$, else $\delta_{k,j} = 0$) and $\boldsymbol{Q}_k$ is the covariance matrix of $\boldsymbol{w}_{t;k}$. The covariance matrix can be derived as [11]

$$\begin{aligned}\boldsymbol{Q}_k &\triangleq \mathrm{cov}(\boldsymbol{w}_{t;k}) \\ &= 2\alpha\sigma_t^2 \int\limits_{t_{k-1}}^{t_k} e^{(t_k-\tau)\boldsymbol{F}_{k-1}}\boldsymbol{\Theta}e^{(t_k-\tau)\boldsymbol{F}_{k-1}^T}\mathrm{d}\tau,\end{aligned} \tag{25}$$

where $\boldsymbol{\Theta} \triangleq \boldsymbol{G}\boldsymbol{G}^T$. If the exponential terms in (25) are replaced by their 1st-order Taylor series approximations, i.e.,

$$e^{(t_k-\tau)\boldsymbol{F}_{k-1}} \approx \boldsymbol{I} + (t_k-\tau)\boldsymbol{F}_{k-1},$$
$$e^{(t_k-\tau)\boldsymbol{F}_{k-1}^T} \approx \boldsymbol{I} + (t_k-\tau)\boldsymbol{F}_{k-1}^T,$$

then the integral in (25) can be easily solved and $\boldsymbol{Q}_k$ approximated by

$$\begin{aligned}&\boldsymbol{Q}_k \approx 2\alpha\sigma_t^2 T_d \\ &\times\left[\boldsymbol{\Theta} + \frac{T_d}{2}\left(\boldsymbol{F}_{k-1}\boldsymbol{\Theta}+\boldsymbol{\Theta}\boldsymbol{F}_{k-1}^T\right) + \frac{T_d^2}{3}\boldsymbol{F}_{k-1}\boldsymbol{\Theta}\boldsymbol{F}_{k-1}^T\right],\end{aligned} \tag{26}$$

where $T_d \triangleq t_k - t_{k-1}$ is the discretization sampling time. In this paper, we assume that $T_d = T_s$, where T_s is the measurement sampling time, see Section II-C.

D. Filtering Equations

The system (21) and the measurement (14) equations are nonlinear. Thus, a suitable estimation technique must be considered. In this paper, we will employ an extended Kalman filter (EKF) based approach to obtain an approximate solution to the optimal filtering problem of finding $E\left[\boldsymbol{x}_{m;k}|\boldsymbol{z}_{1:k}\right]$. Other sub-optimal estimation techniques, such as unscented Kalman filter (UKF) or particle filter can be considered. We expect similar trends in the estimation performance, as all these filters have comparable characteristics for similar application [16].

Assuming that at time $t_0 = 0$, an initial estimate, $\hat{\boldsymbol{x}}_{m;0|0}$, of the missile state $\boldsymbol{x}_{m;0}$ is available, satisfying

$$\hat{\boldsymbol{x}}_{m;0|0} \sim \mathcal{N}\left(\boldsymbol{x}_{m;0}, \boldsymbol{P}_{0|0}\right), \tag{27}$$

where $\boldsymbol{P}_{0|0}$ is the covariance matrix of the initial estimation error ($\boldsymbol{x}_{m;0}-\hat{\boldsymbol{x}}_{m;0|0}$), then the filtering process can be divided into two steps of time propagation (TP) and measurement update (MU).

TP: The a posteriori state estimate $\hat{\boldsymbol{x}}_{m;k-1|k-1}$ is time-propagated from t_{k-1} to t_k using

$$\hat{\boldsymbol{x}}_{m;k|k-1} = \boldsymbol{f}_{k-1}^d(\hat{\boldsymbol{x}}_{m;k-1|k-1}), \tag{28}$$

where $\boldsymbol{f}_{k-1}^d(\cdot)$ was defined shortly after (21). The a posteriori covariance matrix $\boldsymbol{P}_{k-1|k-1}$ is propagated using

$$\boldsymbol{P}_{k|k-1} = e^{\boldsymbol{F}_{k-1}T_d}\boldsymbol{P}_{k-1|k-1}e^{\boldsymbol{F}_{k-1}^T T_d} + \boldsymbol{Q}_k, \tag{29}$$

where $\boldsymbol{Q}_k$ is given in (26) and $\boldsymbol{F}_{k-1}$ is the Jacobian matrix (23) evaluated at $\boldsymbol{x}_m = \hat{\boldsymbol{x}}_{m;k-1|k-1}$.

MU: If the measurement z_k becomes available at time t_k, the a priori state estimate $\hat{\boldsymbol{x}}_{m;k|k-1}$ is updated using

$$\hat{\boldsymbol{x}}_{m;k|k} = \hat{\boldsymbol{x}}_{m;k|k-1} + \boldsymbol{K}_k\left[z_k - h_w(\hat{\boldsymbol{x}}_{m;k|k-1}, \boldsymbol{\phi}_k)\right], \tag{30}$$

where $h_w(\cdot,\cdot)$ was defined in (11) and $\boldsymbol{K}_k$ is the Kalman gain computed as

$$\boldsymbol{K}_k = \boldsymbol{P}_{k|k-1}\boldsymbol{H}_k^T\left(\boldsymbol{H}_k\boldsymbol{P}_{k|k-1}\boldsymbol{H}_k^T + R\right)^{-1}. \tag{31}$$

In (31), R stands for the variance of the measurement noise v_k, i.e., $R = \sigma_{\lambda,w}^2$, and $\boldsymbol{H}_k$ is the Jacobian of the measurement model (11), derived as

$$\begin{aligned}\boldsymbol{H}_k &\triangleq \left.\frac{\partial h_w(\boldsymbol{x}_m, \boldsymbol{\phi})}{\partial \boldsymbol{x}_m}\right|_{\boldsymbol{x}_m=\hat{\boldsymbol{x}}_{m;k|k-1},\ \boldsymbol{\phi}=\boldsymbol{\phi}_k} \\ &= \left.\begin{bmatrix}H_1 & H_2 & 0 & 0 & 0\end{bmatrix}\right|_{\boldsymbol{x}_m=\hat{\boldsymbol{x}}_{m;k|k-1},\ \boldsymbol{\phi}=\boldsymbol{\phi}_k},\end{aligned} \tag{32}$$

with H_1 and H_2 being defined as

$$H_1 = +s\frac{r\sqrt{|\cos^2(\lambda-\lambda_m)-1|}}{g_w^2\left(\hat{\boldsymbol{x}}_{m;k|k-1}, \boldsymbol{\phi}_k\right)},$$
$$H_2 = s\frac{rr_m\sin(2\lambda-2\lambda_m)+2r_m^2\sin(\lambda-\lambda_m)}{2g_w^2\left(\hat{\boldsymbol{x}}_{m;k|k-1}, \boldsymbol{\phi}_k\right)\sqrt{|\cos^2(\lambda-\lambda_m)-1|}},$$

where $g_w(\cdot,\cdot)$ and s were defined in (12) and (13), respectively. The values of r_m, r, λ_m, and λ in H_1 and H_2 are substituted with corresponding entries from $\hat{\boldsymbol{x}}_{m;k|k-1}$ and $\boldsymbol{\phi}_k$. The a priori covariance matrix $\boldsymbol{P}_{k|k-1}$ is updated as

$$\boldsymbol{P}_{k|k} = \boldsymbol{P}_{k|k-1} - \boldsymbol{K}_k\boldsymbol{H}_k\boldsymbol{P}_{k|k-1}. \tag{33}$$

Note that to compute (30) and (32), the sign function s, defined in (13), needs to be evaluated. It requires the knowledge of $\lambda_{w;k}$. This angle is not precisely known, but is directly measured, see (8). Thus, for practical implementation purposes, $\lambda_{w;k}$ in (13) can be replaced by z_k or, better yet, by its a priori estimate $\hat{\lambda}_{w;k|k-1} = h_w(\hat{\boldsymbol{x}}_{m;k|k-1}, \boldsymbol{\phi}_k)$.

Remark 3. *To compute an estimate of $\boldsymbol{x}_{m;k}$ using the missile own-ship LOS angle measurements, only slight modifications to the above equations are necessary. The indirect measurement model $h_w(\cdot,\cdot)$ in (30) is replaced by $h(\boldsymbol{x}_m) \triangleq \lambda_m$, the measurement Jacobian $\boldsymbol{H}_k$ simplifies to $\boldsymbol{H}_k = \begin{bmatrix}0 & 1 & 0 & 0 & 0\end{bmatrix}$, and R in (31) is set to $R = \sigma_{\lambda,m}^2$, where $\sigma_{\lambda,m}^2$ is the variance of the missile's sensor noise.*

Remark 4. *The proposed wingman-based estimation scheme can be extended with a little extra effort to a multiple wingman-based measuring scheme. This can be accomplished by transforming all measurements from the wingmans' to the missile's moving frame and fusing them similarly as in [17].*

IV. Observability Analysis

In this section, we will analytically study the accuracy of the wingman-based estimation concept developed in the previous section.

This article has been accepted for publication in a future issue of this journal, but has not been fully edited. Content may change prior to final publication. Citation information: DOI 10.1109/TAES.2019.2935642, IEEE Transactions on Aerospace and Electronic Systems

A. Observability Metrics Derivation

The estimation accuracy of a_t, γ_t, and V_t is mainly driven by the availability of an accurate target maneuver model, and the actual target maneuvers. Moreover, as will be discussed in the next section, the accuracy of these parameters is not very crucial for the implementation of the PN guidance law of (10). Therefore, the focus of this section will be only on the observability of λ_m and r_m.

We will investigate the observability of λ_m and r_m from a geometric perspective. Consider the engagement geometry depicted in Fig. 1. From the law of cosines, the M–T range can be expressed as

$$r_m = g_m(r_w, \lambda_w, \boldsymbol{\phi}) \triangleq \sqrt{r^2 + r_w^2 - 2rr_w \cos\Delta_\lambda}, \tag{34}$$

where Δ_λ is defined as the difference between the W–M and W–T LOS angles, i.e.,

$$\Delta_\lambda \triangleq \lambda - \lambda_w. \tag{35}$$

Inserting r_m of (34) in the expression of r_w given in (12), we can easily isolate λ_m as follows

$$\lambda_m = h_m(r_w, \lambda_w, \boldsymbol{\phi}) \triangleq \lambda + \cos^{-1}\left(\frac{r - r_w\cos\Delta_\lambda}{g_m\left(r_w, \lambda_w, \boldsymbol{\phi}\right)}\right). \tag{36}$$

The above expressions of r_m and λ_m will form the baseline for the subsequent observability analysis.

To proceed, we need to take into account the stochastic nature of the measurements and the state estimate. Consider that, at time step k, r_w in (34) and (36) is replaced by its a priori state estimate, i.e.,

$$\hat{r}_{w;k} = g_w\left(\hat{\boldsymbol{x}}_{m;k|k-1}, \boldsymbol{\phi}_k\right) = r_{w;k} + v_{r_w;k}. \tag{37}$$

In this context, $\hat{r}_{w;k}$ is viewed as a random variable, where $v_{r_w;k}$ is assumed to be a zero-mean random process with a time-varying variance $\sigma^2_{r,w;k}$. Note that expression (37) is the same as the one used at the MU stage of the EKF, see $h_w(\cdot,\cdot)$ in (30) and (32). In both cases, $r_{w;k}$ is evaluated using the a priori state estimate $\hat{\boldsymbol{x}}_{m;k|k-1}$ and the definition of $g_w(\cdot,\cdot)$ given in (12). Consequently, the accuracy of $\hat{r}_{w;k}$ will be driven by the filter's performance, i.e., $\sigma^2_{r,w;k}$ is essentially a function of $\boldsymbol{P}_{k|k-1}$.

For observability analysis purposes, λ_w in (34) and (36) is replaced by the wingman's noise-corrupted measurement $z_k = \lambda_{w;k} + v_{\lambda_w;k}$. Consider that the accuracy of $\hat{r}_{w;k}$ and z_k is quantified by their standard deviations $\sigma_{r,w;k}$ and $\sigma_{\lambda,w}$, respectively, then

$$\lambda^\dagger_{m;k} = h_m\left(\hat{r}_{w;k}, z_k, \boldsymbol{\phi}_k\right), \tag{38a}$$
$$r^\dagger_{m;k} = g_m\left(\hat{r}_{w;k}, z_k, \boldsymbol{\phi}_k\right), \tag{38b}$$

can be viewed as pseudomeasurements of $\lambda_{m;k}$ and $r_{m;k}$, respectively.

Next, the accuracy of the above pseudomeasurements will be analyzed. Because $\hat{r}_{w;k}$ in (38) is expressed using the a priori state estimate $\hat{\boldsymbol{x}}_{m;k|k-1}$, the two random processes of $v_{r_w;k}$ and $v_{\lambda_w;k}$ are mutually independent, i.e., $E\left[v_{r_w;k}, v_{\lambda_w;k}\right] = 0$. Therefore, the associated variance of the LOS angle pseudomeasurement, $\lambda^\dagger_{m;k}$, can be exactly computed, as

$$\begin{aligned}\sigma^2_{\lambda,m;k} = \int\limits_{\mathbb{R}^2} &\Big[\left(h_m(\hat{r}_{w;k}, z_k, \boldsymbol{\phi}_k) - \mu_{\lambda,m;k}\right)^2 \\ &\times f_r(v_{r_w}) f_\lambda(v_{\lambda_w})\Big]\, \mathrm{d}v_{r_w}\mathrm{d}v_{\lambda_w},\end{aligned} \tag{39}$$

where $\mu_{\lambda,m;k}$ is the mean value of $\lambda^\dagger_{m;k}$,

$$\mu_{\lambda,m;k} = \int\limits_{\mathbb{R}^2} h_m(\hat{r}_{w;k}, z_k, \boldsymbol{\phi}_k) f_r(v_{r_w}) f_\lambda(v_{\lambda_w}) \mathrm{d}v_{r_w}\mathrm{d}v_{\lambda_w}, \tag{40}$$

and $f_r(\cdot)$ and $f_\lambda(\cdot)$ are two scalar Gaussian density functions with zero means and variances $\sigma^2_{r,w;k}$ and $\sigma^2_{\lambda,w}$, respectively. In a similar manner, the variance of $r^\dagger_{m;k}$, denoted as $\sigma^2_{r,m;k}$, can be computed using the relations above with $h_m(\cdot,\cdot,\cdot) \to g_m(\cdot,\cdot,\cdot)$.

Unfortunately, the integrals in (39) and (40) are not trivial to compute. Hence, in this paper, we will attempt to solve these integrals by the *analytical linearization* (AL) technique [18]. The AL, also used in the EKF algorithm derivation, aims at obtaining the variance of the transformed random variable(s) using linearization of the underlying nonlinear function and evaluating at expected values. Thus, the variance of the M–T LOS angle pseudomeasurement, $\lambda^\dagger_{m;k}$, obtained using the AL method, becomes

$$\begin{aligned}\sigma^2_{\lambda,m;k} &\approx \sigma^2_{r,w;k}\left(\frac{\partial h_m(\hat{r}_w, z, \boldsymbol{\phi}_k)}{\partial \hat{r}_w}\right)^2\Bigg|_{\hat{r}_w = E[\hat{r}_{w;k}],\, z = E[z_k]} \\ &\quad + \sigma^2_{\lambda,w}\left(\frac{\partial h_m(\hat{r}_w, z, \boldsymbol{\phi}_k)}{\partial z}\right)^2\Bigg|_{\hat{r}_w = E[\hat{r}_{w;k}],\, z = E[z_k]} \\ &= \sigma^2_{r,w;k}\left(\frac{r\sin\Delta_\lambda}{g_m^2(r_w, \lambda_w, \boldsymbol{\phi})}\right)^2 + \sigma^2_{\lambda,w}\left(\frac{rr_w\cos\Delta_\lambda - r_w^2}{g_m^2(r_w, \lambda_w, \boldsymbol{\phi})}\right)^2.\end{aligned} \tag{41}$$

Similarly, using AL, the variance of the M–T range pseudomeasurement, $r^\dagger_{m;k}$, becomes

$$\begin{aligned}\sigma^2_{r,m;k} &\approx \sigma^2_{r,w;k}\left(\frac{\partial g_m(\hat{r}_w, z, \boldsymbol{\phi}_k)}{\partial \hat{r}_w}\right)^2\Bigg|_{\hat{r}_w = E[\hat{r}_{w;k}],\, z = E[z_k]} \\ &\quad + \sigma^2_{\lambda,w}\left(\frac{\partial g_m(\hat{r}_w, z, \boldsymbol{\phi}_k)}{\partial z}\right)^2\Bigg|_{\hat{r}_w = E[\hat{r}_{w;k}],\, z = E[z_k]} \\ &= \sigma^2_{r,w;k}\left(\frac{r\cos\Delta_\lambda - r_w}{g_m(r_w, \lambda_w, \boldsymbol{\phi})}\right)^2 + \sigma^2_{\lambda,w}\left(\frac{rr_w\sin\Delta_\lambda}{g_m(r_w, \lambda_w, \boldsymbol{\phi})}\right)^2.\end{aligned} \tag{42}$$

The analytical expressions of (41) and (42) provide powerful means to analyze the observability of λ_m and r_m as a function of the W–M relative geometry.

B. Observability Metrics' Verification and Analysis

The AL method is often criticized to give inaccurate results. Therefore, we will verify the analytical results of (41) and (42) using a *Monte Carlo* (MC) statistical method. Unlike AL, the MC method does not yield an explicit solution for the variance of the transformed random variable(s), but instead uses sufficiently large number of realizations of the random variable(s) to numerically approximate the underlying distribution. This method reassembles the unscented transformation used in the UKF. Here, instead of using only few "sigma points", a large number, N, of realizations is generated from the prior distribution of $\hat{r}_{w;k} \sim \mathcal{N}(r_{w;k}, \sigma^2_{r,w;k})$ and $z_k \sim \mathcal{N}(\lambda_{w;k}, \sigma^2_{\lambda,w})$, which are then propagated through the nonlinear functions $h_m(\cdot,\cdot,\cdot)$ and $g_m(\cdot,\cdot,\cdot)$, and the sample variances are computed:

$$\sigma^2_{\lambda,m;k} \approx \frac{1}{N-1}\sum_{i=1}^{N}\left(\lambda^{\dagger(i)}_{m;k} - \frac{1}{N}\sum_{j=1}^{N}\lambda^{\dagger(j)}_{m;k}\right)^2, \tag{43a}$$

$$\sigma^2_{r,m;k} \approx \frac{1}{N-1}\sum_{i=1}^{N}\left(r^{\dagger(i)}_{m;k} - \frac{1}{N}\sum_{j=1}^{N}r^{\dagger(j)}_{m;k}\right)^2, \tag{43b}$$

where the superscript "i" denotes the ith realization of the pseudomeasurement $\lambda^\dagger_{m;k}$ or $r^\dagger_{m;k}$.

Without loss of generality, for the subsequent analysis, we will assume that $\sigma_{r,w;k}$ is constant, i.e., $\sigma_{r,w;k} = \sigma_{r,w}$ for all $k \in \mathbb{N}$ and that $r_w > 0$. The constant $\sigma_{r,w}$ assumption can be viewed as a worst-case uncertainty for r_w, i.e., $\sigma_{r,w;k} \leq \sigma_{r,w}$, $\forall k \in \mathbb{N}$. The normalized values of $\sigma_{\lambda,m}$ and $\sigma_{r,m}$ are depicted in Fig. 4 for different W–M angle separations Δ_λ and ranges r. The obtained results are normalized by $\sigma_{\lambda,w} = 0.001$ and $\sigma_{r,w} = r_w/100$ to better appreciate the relative uncertainty change with respect to these reference uncertainties. The W–M range, r, is made dimensionless by r_w. For the MC method, a total number of $N = 1,000,000$ points were generated for each Δ_λ and r/r_w combination, see the circles in Fig. 4. It can be observed that the AL method very closely matches with the MC method. To reflect on Assumption 4, the infeasible W–M relative geometries are depicted as filled circles. These regions represent unfavourable W–M geometries when, for a given Δ_λ, the wingman is closer to the target than the missile ($r_w < r_m$). Note that the trends depicted in Fig. 4 are particular for the considered values of $\sigma_{\lambda,w}$ and $\sigma_{r,w}$ in this analysis.

It can be observed from Fig. 4, that if the position of the missile and the wingman coincide, i.e., $r = 0 \Rightarrow r/r_w = 0$, the estimation accuracy of λ_m will be purely driven by the accuracy of the wingman's measurements $\sigma_{\lambda,w}$ and $\sigma_{r,m} = \sigma_{r,w}$ for any Δ_λ. This is obvious as this case is identical to a missile having own-ship measurements with accuracy of $\sigma_{\lambda,w}$. However, if the wingman and the missile are apart, i.e., $r/r_w > 0$, a contradictory behavior in the estimation accuracy of the M–T kinematic variables (range r_m and LOS angle λ_m) can be observed for $|\Delta_\lambda| \to 0$. While for $\Delta_\lambda = 0$, the observability of the M–T line-of-sight angle λ_m is maximized, the observability of the M–T range r_m is minimized. Similarly, increasing $|\Delta_\lambda|$, opposing trends can be observed for $\sigma_{\lambda,m}$ vs. $\sigma_{r,m}$. Increasing r/r_w leads to improving accuracy of r_m w.r.t. the accuracy of r_w. This trend can be explained by the fact that increasing r/r_w means that the missile is approaching the target and the accurately known W–M relative position (r, λ) has an improving effect on the M–T range estimate as the accuracy of the approximation

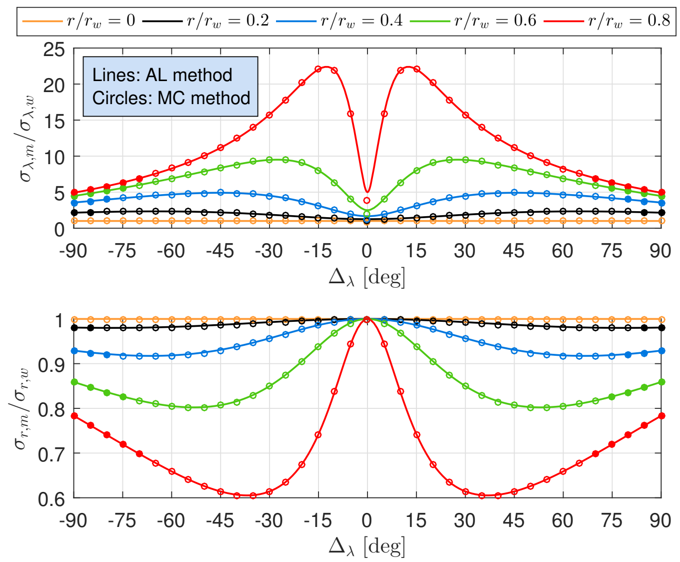

Fig. 4. Effect of W–M relative geometry on the M–T range and LOS angle accuracy

$r_m \approx r\sin(\lambda - \lambda_w)$ becomes more and more valid. Note that both r and λ are assumed to be known and λ_w is directly measured.

Figure 4 presents a rather static grasp of the underlying observability issue. Next, we will attempt to address some dynamical aspects of the considered engagement scenario. Based on Assumption 4, we have $r_m(t_0) = r_w(t_0)$ at the beginning of the engagement, thus $r(t_0) = 0$. In a perfect interception scenario, $r_m(t_f) = 0$. This implies $r(t_f) = r_w(t_f) > 0$. Considering Assumption 4 again, it becomes evident that $r(t)/r_w(t)$ is continuous and monotonously increasing from 0 to 1 on the interval $t \in \langle t_0, t_f \rangle$, hence takes values exclusively in the closed interval $\langle 0, 1\rangle$. This insight enables us to parameterize (41) and (42) for all, feasible and infeasible, engagement trajectories by considering ($r_w > 0$)

$$-\pi/2 \leq \Delta_\lambda \leq \pi/2, \qquad 0 \leq r/r_w < 1. \tag{44}$$

Next, we are only interested in the feasible LOS separation angles Δ_λ which minimize $\sigma^2_{\lambda,m}$ and $\sigma^2_{r,m}$, respectively, for a given ratio r/r_w. This can be mathematically formulated as:

$$\Delta^{min}_\lambda(r/r_w) = \underset{|\Delta_\lambda| \leq \bar{\Delta}_\lambda}{\operatorname{argmin}} \left\{\sigma^2_{j,m}\right\}, \quad j \in \{\lambda, r\}. \tag{45}$$

where $\bar{\Delta}_\lambda = \cos^{-1}(r/r_w)$ is the maximal feasible LOS separation angle for a given r/r_w ratio. The resulting angles Δ^{min}_λ for $0 \leq r/r_w < 1$ are depicted in Fig. 5. Absolute value is used for the y-axis as $\sigma^2_{\lambda,m}$ and $\sigma^2_{r,m}$ are symmetric functions around $\Delta_\lambda = 0$ [deg], see Fig. 4. Note that the limit case $r/r_w = 1$ yields to singularity issues in (41) and (42) and is also not relevant from observability perspective as $r/r_w = 1$ occurs only at the end of the engagement when $r_m(t_f) = 0$, therefore $r/r_w = 1$ is considered only as a limit in Fig. 5. Again, the results obtained by the AL method are verified by the MC method using (43).

It becomes evident from Fig. 5 that simultaneous minimization of uncertainties associated with both λ_m and r_m is not

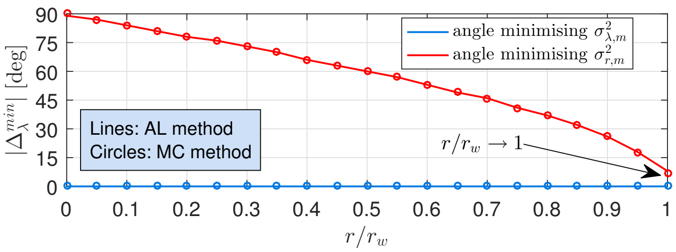

Fig. 5. LOS separation angles Δ_λ minimizing uncertainties in the M–T range and LOS angle.

possible. Moreover, keeping Δ_λ close to zero will on one hand minimize $\sigma^2_{\lambda,m}$ for all $0 \leq r/r_w < 1$, but on the other hand will maximize $\sigma^2_{r,m}$, see the lower subfigure in Fig. 4 for $\Delta_\lambda = 0$ [deg].

Remark 5. *Further research is needed to fully understand the practical implications of the observed variations of $\sigma_{r,m}$ and of $\sigma_{\lambda,m}$ w.r.t. that of Δ_λ and/or r/r_w.*

V. Wingman Trajectory Implications

Based on the preceding observability analysis, possible wingman trajectory implications are discussed in this section.

A. Wingman Trajectory Implications for a PN-Guided Missile

The trajectory of the missile is predetermined by the employed PN guidance law (10), therefore the focus of this section will be on the remaining degree of freedom, which is the choice of the wingman's trajectory. The resulting wingman trajectory should maximize the missile's homing performance.

To implement the PN guidance law (10), only the missile-target LOS angle rate $\dot{\lambda}_m$ and the closing velocity $V_{c,m}$ shall be provided. The closing velocity is typically assumed to be constant throughout the endgame and can be easily computed using the estimated state $\hat{\boldsymbol{x}}_m$. However, absence of an accurate estimate on $V_{c,m}$, in general, does not significantly affect the homing performance of a PN-guided missile.

On the other hand, an effective implementation of the PN guidance law requires accurate information on the LOS rate $\dot{\lambda}_m$ [19]. In a typical one-on-one M–T engagement, this is accomplished by directly measuring the LOS angle λ_m or the LOS angle rate $\dot{\lambda}_m$. Therefore, in such a scenario, the estimation accuracy of the LOS angle (rate) is directly governed by the accuracy of the sensor(s) measurements. However, in the proposed wingman-based estimation scheme, only the LOS angle λ_w of the W–T engagement is measured. The accuracy of the λ_w measurement is only indirectly related to the M–T LOS angle (rate), see λ_m and λ_w in (36).

Direct knowledge on the target acceleration a_t is not required for the PN guidance law implementation, but a_t must be included in $\boldsymbol{x}_m$ to enable estimation of γ_t, which is, together with V_t, essential for estimating r_m and λ_m, see (1).

Based on the above discussion, it might seem natural for the wingman to try to maximize the observability of the M–T LOS angle λ_m, as this is the most critical variable for the PN guidance law implementation. Figure 5 clearly suggests that in order to maximize the observability of λ_m, the relative LOS separation Δ_λ must be kept zero throughout the entire engagement. This leads to a straightforward formulation of the wingman's trajectory, which is to maintain Δ_λ zero at all times, i.e.,

$$\Delta_\lambda(t) = 0, \qquad \forall t \in \langle t_0, t_f \rangle. \tag{46}$$

B. Wingman's Guidance Law Implementation

Consider the desired wingman trajectory described in terms of (46) and the simplified engagement geometry depicted in Fig. 6. It becomes evident that the wingman's guidance problem can be related to the well known LOS guidance concept in a three-body engagement. Its basic principle is to keep a pursuer on the LOS connecting a target and a (stationary) launch platform. In our case, the missile can be conceptually regarded as the moving launch platform and the wingman tries to maintain its position on the extended M–T LOS line. This guidance problem can be also considered in the framework of the target-attacker-defender problem [20], [21], which is another three-point problem, where a defender missile aids a target to negate the threat from an attacking missile.

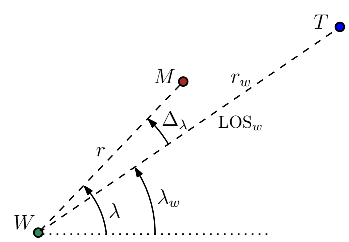

Fig. 6. Three-point guidance problem visualization.

The mechanization of the "classical" three-point LOS guidance problem is commonly achieved by implementing either command to LOS (CLOS) or beam rider LOS (BR-LOS) guidance law [19]. The physical implementation of BR-LOS is conceptually not feasible due to geometrical constraints resulting from Assumption 4 (wingman flying behind the missile). In a conventional CLOS guidance, the launcher computes the guidance command and sends it to the pursuer for execution. In our case, the "pursuer" computes the guidance command and also executes it itself. While the CLOS guidance law is conceptually feasible, it was devised for a stationary launch platform. A CLOS guidance problem with a moving/maneuvering launch platform was studied in [21], where a defender missile implemented a LOS guidance concept to maintain its position on the LOS connecting the targeted aircraft with the homing missile. Nevertheless, the CLOS-based guidance law implementation would require accurate knowledge of r, $\dot{r}$, λ_m, $\dot{\lambda}_m$, and $\ddot{\lambda}_m$. The approach presented in [21], in addition, would require the knowledge of a_t. Although, most of these variables are assumed to be known (r), estimated (λ_m and a_t), or can be obtained by numerical differentiation ($\dot{r}$, $\dot{\lambda}_m$, and $\ddot{\lambda}_m$), we did not select CLOS as a candidate for solving our guidance problem formulated by (46). This is because λ_m is not directly measured in the proposed concept and, as discussed in Section IV, its estimation accuracy is determined by the actual wingman trajectory. Therefore, the accuracy of λ_m, $\dot{\lambda}_m$, and $\ddot{\lambda}_m$ may severely limit the wingman's ability to accurately maintain the extended M–T LOS line, thus limit the homing performance of the missile.

Ideally, the wingman's guidance law should not directly depend on λ_m or on any of its derivatives. Perhaps the simplest mechanization of the wingman's guidance law is by employing a discrete-time proportional-integral-derivative (PID) controller to minimize the error represented by the LOS separation angle $\Delta_\lambda = \lambda - \lambda_w$. The discrete-time implementation of such a PID-based LOS (PLOS) guidance strategy takes the following structure:

$$u_{w;k} = K_p\hat{\Delta}_{\lambda;k} + K_i T \sum_{j=0}^{k} \hat{\Delta}_{\lambda;j} + K_d \frac{\hat{\Delta}_{\lambda;k} - \hat{\Delta}_{\lambda;k-1}}{T}, \quad (47)$$

where $u_{w;k}$ is the wingman's commanded lateral acceleration at time t_k, $T = t_k - t_{k-1}$ is the discretization step, K_p, K_i, K_d are the PID controller's tuning parameters [22], and $\hat{\Delta}_{\lambda;k}$ is the estimate of $\Delta_{\lambda;k} = \lambda_k - \lambda_{w;k}$. If $T = T_s$, then the wingman measurement z_k or the state estimate $\hat{\boldsymbol{x}}_{m;k|k}$ can be used to compute $\hat{\Delta}_{\lambda;k}$ as follows

$$\hat{\Delta}_{\lambda;k} = \lambda_k - z_k, \quad \text{or} \quad \hat{\Delta}_{\lambda;k} = \lambda_k - h_w(\hat{\boldsymbol{x}}_{m;k|k}, \boldsymbol{\phi}_k), \quad (48)$$

where $h_w(\cdot,\cdot)$ was defined in (11). In (48), the use of $h_w(\cdot,\cdot)$ is preferred over z_k, as it reduces sensitivity of $\hat{\Delta}_{\lambda;k}$ to noise.

The PID algorithm of (47) can be written in a recursive form

$$u_{w;k} = u_{w;k-1} + K_1\hat{\Delta}_{\lambda;k} - K_2\hat{\Delta}_{\lambda;k-1} + K_3\hat{\Delta}_{\lambda;k-2}, \quad (49)$$

with $K_1 = K_p + K_i T + K_d/T$, $K_2 = K_p + 2K_d/T$, and $K_3 = K_d/T$. This form of the wingman's guidance law facilitates its on-board implementation. A proper tuning of the PID parameters is important, because a relatively small deviation of Δ_λ from zero leads to a significant deterioration in the estimation accuracy of λ_m, especially at the end of the engagement, see the upper subplot of Fig. 4. Note that (47) or (49) requires only the availability of λ_k and not r_k. Hence Assumption 2 can be slightly relaxed for the proposed PLOS wingman guidance strategy implementation.

Remark 6. *The wingman is expected to fly behind the missile on the extended W–T LOS line. If the wingman does not "see" the target because it is shadowed by the missile then, it knows, with some angular error, at which angle the target is w.r.t. the wingman. This angular error will be smaller as the missile approaches the target.*

C. Other Missile Guidance Laws and Their Implications

The preceding developments assumed PN guidance law for the missile. Obviously, other missile guidance strategies might lead to different (optimal) trajectory implications for the wingman. For instance, the optimal guidance law [23] or the impact time/angle guidance law [24], [25] require an accurate estimation of the time-to-go (t_{go}) variable. The estimation accuracy of t_{go} is highly dependent on the M–T range (r_m) estimate accuracy, see the typical t_{go} approximation in (7).

The W–M engagement parametrization (44) enables to pose the following weighted optimization problem

$$\Delta_\lambda^\star(r/r_w, \varepsilon) = \underset{-\frac{\pi}{2} \le \Delta_\lambda \le \frac{\pi}{2}}{\operatorname{argmin}} \left\{ \varepsilon\sigma_{\lambda,m}^2 + (1-\varepsilon)\sigma_{r,m}^2 \right\}, \quad (50)$$

where $\sigma_{\lambda,m}^2$ and $\sigma_{r,m}^2$ are given in (41) and (42), $0 \le \varepsilon \le 1$ is a weight factor trading the uncertainty between λ_m and r_m, and $\Delta_\lambda^\star$ is the optimal LOS angle between W and M which minimizes the weighted uncertainty for a given ε and r/r_w. The physical interpretation of ε can be difficult due to the fact that $\sigma_{\lambda,m}^2$ and $\sigma_{r,m}^2$ might operate at different magnitudes. Therefore, proper scaling shall be introduced in (50).

By an adequate choice of ε in (50), an optimal wingman trajectory (parameterized in terms of r/r_w and $\Delta_\lambda^\star$) can be obtained, which reflects the estimation accuracy needs for r_m and/or λ_m. These accuracy needs shall be driven by the employed missile guidance strategy and its implementation requirements. The resulting trajectory should then serve as a baseline for the wingman's guidance law derivation, which is out of scope of this paper.

Remark 7. *More sophisticated wingman guidance algorithms might require the availability of the W–T state vector $\boldsymbol{x}_w$, defined in a similar manner as $\boldsymbol{x}_m$, i.e.,*

$$\boldsymbol{x}_w \triangleq \begin{bmatrix} r_w & \lambda_w & \gamma_t & a_t & V_t \end{bmatrix}^T. \quad (51)$$

An estimate of $\boldsymbol{x}_w$ can be easily obtained either by running a separate estimator for the W–T engagement, or by using $\hat{\boldsymbol{x}}_{m;k|k}$ and the following relations

$$\hat{r}_{w;k} = g_w(\hat{\boldsymbol{x}}_{m;k|k}, \boldsymbol{\phi}_k), \qquad \hat{\lambda}_{w;k} = h_w(\hat{\boldsymbol{x}}_{m;k|k}, \boldsymbol{\phi}_k). \quad (52)$$

Estimates on γ_t, a_t, and V_t are contained in $\hat{\boldsymbol{x}}_{m;k|k}$, see (9).

VI. Simulation Results

In this section, numerical simulations are introduced to demonstrate the closed-loop (estimator in the guidance loop) performance of the proposed wingman-based sensorless missile guidance concept. The effect of different wingman guidance strategies and measurement accuracies on the missile homing performance are also presented.

A. Engagement Scenario and Parameters

For all simulations, the missile and the wingman are launched simultaneously from the same initial location. The initial horizontal separation of the target from the wingman–missile team is 5 [km] in the positive X_I direction. The missile and the target are flying with the same constant speed $V_m = V_t = 500$ [m/s] and have first-order lateral dynamics with identical time constants $\tau_m = \tau_t = 0.2$ [s]. The wingman is assumed to fly at a lower speed of $V_w = 400$ [m/s] and to have time constant $\tau_w = 0.05$ [s]. The maximal maneuverability of the target, missile, and the wingman is $a_t^{max} = 5$ [g$_0$], $a_m^{max} = 15$ [g$_0$], and $a_w^{max} = 30$ [g$_0$], respectively. Here, $g_0 = 9.80665$ [m/s^2] represents the standard acceleration due to gravity.

The parameters of the PID-based LOS guidance law were fine tuned to $K_p = 10^5$, $K_d = 5 \cdot 10^6$, and $K_i = 10$. Both, the estimation and guidance loops run at identical sampling rates of 100 [Hz]. The ECA model parameters are set to $\alpha = 1/5$ and $\Psi = \sqrt{5/3}$. The latter corresponds to $P_{\max} = 1$ and $P_0 = 0$, see (16). At each run, the filter's initial state is randomly sampled as

$$\hat{\boldsymbol{x}}_{m;0|0} \sim \mathcal{N}(\boldsymbol{x}_{m;0}, \boldsymbol{P}_{0|0})$$

where $\boldsymbol{x}_{m;0}$ is the true initial state vector defined in (9) and

$$\boldsymbol{P}_{0|0} = \text{diag}\left\{50^2 \quad (\pi/180)^2 \quad (\pi/180)^2 \quad (5\text{g}_0)^2 \quad 25^2\right\}$$

is the initial estimation error covariance matrix of the filter.

B. Sample Run Simulations

Before turning to a statistical MC evaluation, first four sample run examples are presented. In all cases, the wingman (if engaged) acquires bearings-only measurements of the target with $\sigma_{\lambda,w} = 1$ [mrad] accuracy. The missile's navigation constant is $N' = 4$ and the initial flight path angle of the target is $\gamma_{t;0} = 15$ [deg]. Both the missile and the wingman are initially on a perfect collision course with the target, i.e.,

$$\gamma_{j;0} = \sin^{-1}(V_t \sin(\gamma_{t;0} + \lambda_{j;0})/V_j) + \lambda_{j;0}, \quad j \in \{m, w\}.$$

To emulate a realistic interception scenario [26], at first the target applies a constant maneuver turn at $u_t = 5$ [g$_0$] and then, one second before the estimated end of the engagement ($t_{go} = 1$), a maneuver direction switch occurs to the opposite side, i.e., $u_t = -5$ [g$_0$]. Different missile–wingman guidance strategies combinations are demonstrated in Figs. 7–10.

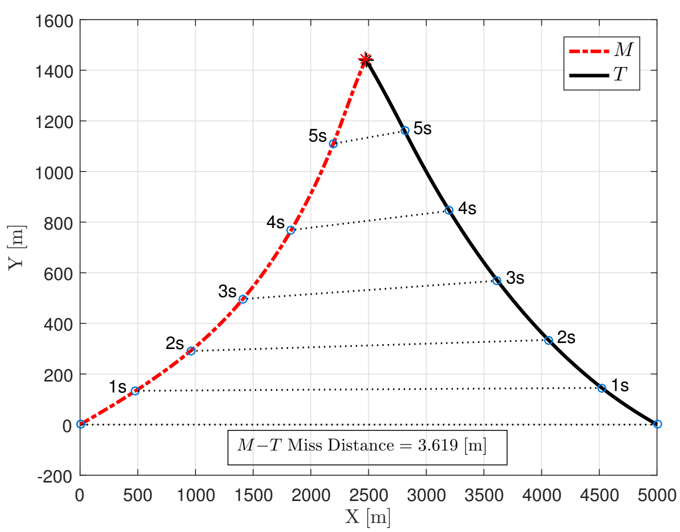

Fig. 7. Missile guided using its own-ship LOS angle measurements.

In Fig. 7, a classical one-on-one scenario is considered, i.e., without the wingman being engaged, where the missile acquires own-ship LOS angle measurements and runs an estimator on its own, designed as described in Remark 3. As expected, a relatively small miss distances is achieved in this case. This is because the accuracy of the M–T LOS angle estimate is directly governed by the accuracy of the missile's own sensory measurements, which in this example were set to $\sigma_{\lambda,m} = 1$ [mrad].

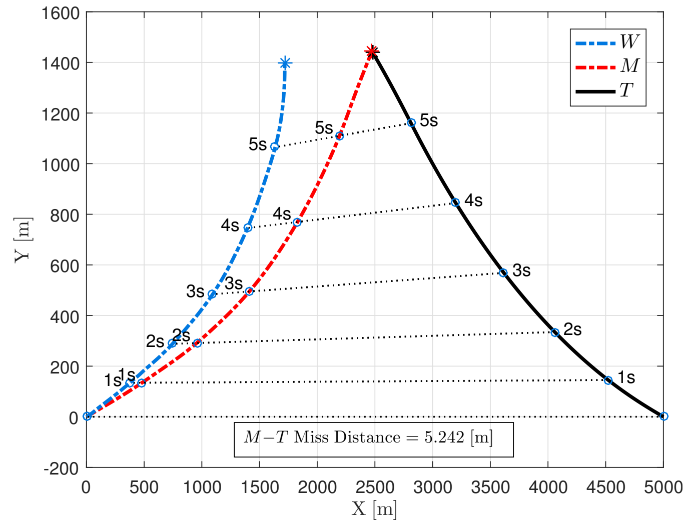

Fig. 8. Sensorless missile guided by the Wingman which employs PLOS guidance law.

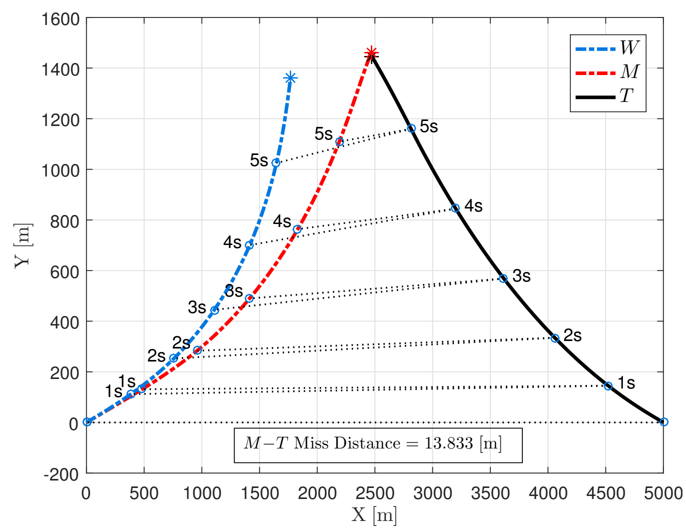

Fig. 9. Sensorless missile guided by the Wingman which employs PN guidance law with $N' = 3$.

The second example, depicted in Fig. 8, considers a sensorless missile being guided by the wingman. The wingman employs the suggested PID-based LOS guidance law of Section V. Thanks to the wingman's agility and its measurements accuracy ($\sigma_{\lambda,w} = 1$ [mrad]), the LOS separation angle Δ_λ is kept close to zero throughout the entire engagement (see the overlaid dotted lines in Fig. 8). The resulting miss is only slightly larger than in the case of the missile having own-ship measurements with the same accuracy.

Fig. 9 demonstrates a case when the W–M relative geometry is similar to that of Fig. 8, but the separation angle Δ_λ is not kept zero throughout the engagement. Here, the wingman employs a PN guidance law (10) with $N' = 3$. The wingman's lateral acceleration command is computed with respect to the W–T LOS and the variables needed for its computation are either assumed to be known (γ_w), are part of the estimated state $\hat{\boldsymbol{x}}_m$, or can be calculated using (52). The

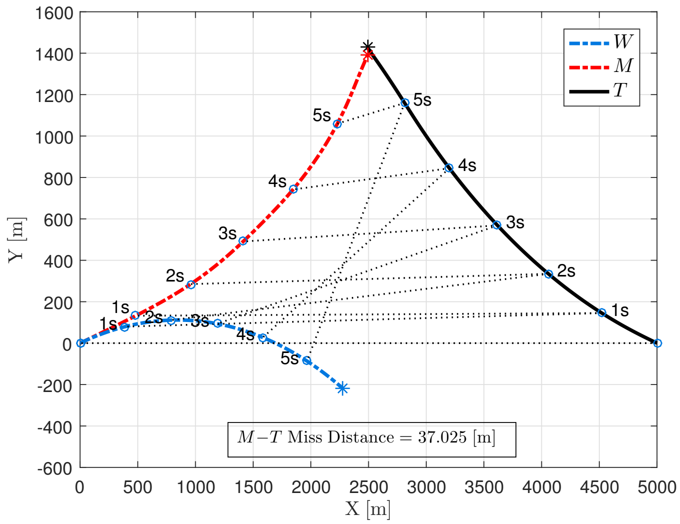

Fig. 10. Sensorless missile guided by the Wingman which performs a single direction maneuver at 5 [g_0].

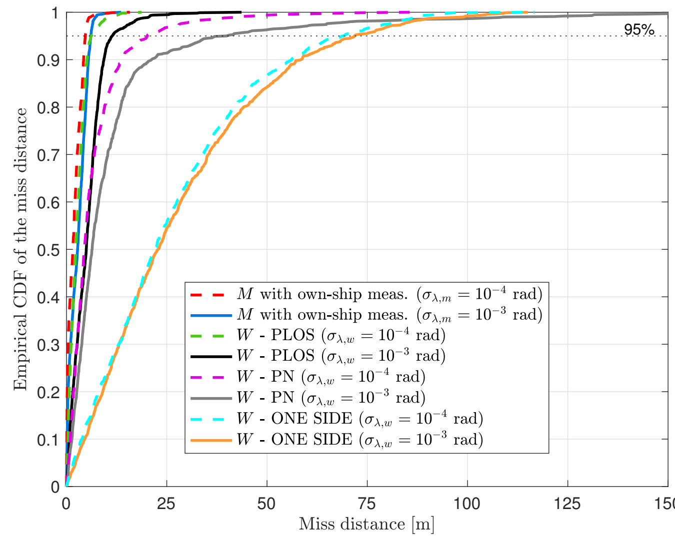

Fig. 11. CDF of the missile-target miss distance for each considered case.

obtained M–T miss is inferior to the preceding two cases. This result emphasizes the importance of Δ_λ being zeroed by the wingman, see the upper plot in Fig. 4 for non-zero Δ_λ angles.

The last example considers a scenario where the wingman performs an acceleration maneuver of 5 [g_0] to the opposite side of the target's flight direction. The obtained trajectories are shown in Fig. 10. The results indicate very poor homing performance of the sensorless missile. This might come as a consequence of poor M–T relative state estimate. Notice that the relative W–M geometry does not follow any of the two optimal relative geometries suggested by Fig. 5.

C. Monte Carlo Simulation Results

The four missile–wingman guidance strategy combinations from the previous subsection are further evaluated here using an extensive Monte Carlo campaign. Furthermore, two different levels of noise intensities are investigated, namely $\sigma_\lambda \in \{0.1, 1\}$ [mrad]. A set of 1,000 MC simulations is run for each case. For each run, the target's initial flight path angle is drawn uniformly from the closed interval $\langle 0, 20\rangle$ [deg]. The initial flight path angles of the missile and the target have a 2 [deg] heading error from the perfect collision course. These heading errors are uniformly distributed. The target's 5 [g_0] maneuver direction switch occurs uniformly between zero and two seconds before the end of the engagement. The missile's navigation gain is selected uniformly from $\{3, 4, 5\}$.

Figure 11 presents the empirical cumulative distribution function (CDF) of the M–T miss distance for each considered case. Table I compiles the obtained results in terms of the warhead lethal range ensuring a 95% kill probability (CDFs' cross point values with the dotted horizontal line in Fig. 11). The obtained MC results reaffirm the sample run results of Figs. 7-10. The results are also in line with the wingman guidance law implications discussed in Sec. V, i.e., the "best" wingman guidance strategy to maximize the sensorless missile homing performance is to employ the suggested PLOS guidance. It is interesting to observe that, in order for the wingman-missile team to achieve similar homing performance as in the traditional one-on-one engagement, the wingman shall have an order of magnitude better LOS measurements.

Sensor accuracy	M only	W-PLOS	W-PN	W-SIDE
$\sigma_\lambda = 10^{-4}$ [rad]	4.71	6.19	20.15	71.78
$\sigma_\lambda = 10^{-3}$ [rad]	6.06	11.33	39.97	68.91

TABLE I
MISSILE'S HOMING PERFORMANCE IN 95% OF RUNS (IN METERS)

VII. CONCLUDING REMARKS

A novel wingman-based estimation and guidance concept for a sensorless PN-guided homing missile was proposed. This concept is based on a wingman vehicle that tracks the target's motion using bearings-only measurements and guides the pursuing missile into collision with a maneuvering aerial target. Only the wingman is assumed to be equipped with sensors that allow to track the target motion and the relative position between the missile and the wingman. The proposed concept enables reduction of weight, on-board computational requirements, and costs for a pursuing missile.

Observability analysis of the wingman-based estimation concept suggests that, in order to achieve maximum observability of the missile–target LOS angle (known to be crucial for a PN-guided missile), the wingman shall fly at a predefined trajectory with respect to the missile. This resulting trajectory can be related to the well-known LOS guidance concept. Implementation aspects of the resulting three-point guidance problem were discussed in the framework of the proposed missile-wingman-target scenario.

Monte Carlo simulation results verified the analytical findings and revealed that, the wingman, when employing the suggested PID-based LOS guidance law, shall have an order of magnitude better bearings-only measurements in order to achieve similar homing performance as the conventional own-ship measurement approach. Different wingman trajectories might lead to better range observability due to rotating wingman-target LOS, however, simulation results revealed that they significantly deteriorate the homing accuracy of a PN-guided missile, which is less sensitive to range errors.

In this work, only the PN-guided missile was analyzed. Other missile guidance laws may be more sensitive to estimation errors in other kinematic variables, and hence different guidance strategies for the wingman shall be considered. The homing accuracy of the sensorless missile could be further improved by introducing additional sensors for the wingman vehicle, such as radar measuring the wingman–target range. Furthermore, the proposed approach could be extended to a shoot-look-shoot strategy where, based on the kill assessment of the missile, the wingman could be actively engaged in the pursuit.

ACKNOWLEDGMENT

This effort was sponsored by the U.S. Air Force Office of Scientific Research, Air Force Materiel Command, under grant number FA9550-15-1-0429. The U.S. Government is authorized to reproduce and distribute reprints for Governmental purpose notwithstanding any copyright notation thereon.

REFERENCES

[1] N. Dhananjay and D. Ghose, "Accurate time-to-go estimation for proportional navigation guidance," *Journal of Guidance, Control, and Dynamics*, vol. 37, no. 4, pp. 1378–1383, 2014.

[2] L. C. Yuan, "Homing and navigational courses of automatic target seeking devices," *Journal of Applied Physics*, vol. 19, no. 12, pp. 1122–1128, 1948.

[3] T. L. Song and T. Y. Um, "Practical guidance for homing missiles with bearings-only measurements," *IEEE Trans. Aerosp. Electron. Syst.*, vol. 32, no. 1, pp. 434–443, 1996.

[4] Y. Oshman and P. Davidson, "Optimization of observer trajectories for bearings-only target localization," *IEEE Trans. Aerosp. Electron. Syst.*, vol. 35, no. 3, pp. 892–902, 1999.

[5] T.-H. Kim, C.-H. Lee, and M.-J. Tahk, "Time-to-go polynomial guidance with trajectory modulation for observability enhancement," *IEEE Trans. Aerosp. Electron. Syst.*, vol. 49, no. 1, pp. 55–73, 2013.

[6] S. Battistini and T. Shima, "Differential games missile guidance with bearings-only measurements," *IEEE Trans. Aerosp. Electron. Syst.*, vol. 50, no. 4, pp. 2906–2915, 2014.

[7] M.-G. Seo and M.-J. Tahk, "Observability analysis and enhancement of radome aberration estimation with line-of-sight angle-only measurement," *IEEE Trans. Aerosp. Electron. Syst.*, vol. 51, no. 4, pp. 3321–3331, 2015.

[8] I.-S. Jeon, J.-I. Lee, and M.-J. Tahk, "Homing guidance law for cooperative attack of multiple missiles," *Journal of Guidance, Control, and Dynamics*, vol. 33, no. 1, pp. 275–280, 2010.

[9] S. Ghosh, D. Ghose, and S. Raha, "Unified time-to-go algorithms for proportional navigation class of guidance," *Journal of Guidance, Control, and Dynamics*, vol. 39, no. 6, pp. 1188–1205, 2016.

[10] R. A. Singer, "Estimating optimal tracking filter performance for manned maneuvering targets," *IEEE Trans. Aerosp. Electron. Syst.*, vol. AES-6, no. 4, pp. 473–483, 1970.

[11] Y. Bar-Shalom, X. R. Li, and T. Kirubarajan, *Estimation with applications to tracking and navigation: theory algorithms and software*. New York, NY: John Wiley & Sons, Inc., 2001.

[12] X. R. Li and V. Jilkov, "Survey of maneuvering target tracking. Part I: Dynamic models," *IEEE Trans. Aerosp. Electron. Syst.*, vol. 39, no. 4, pp. 1333–1364, 2003.

[14] P. Zarchan, "Representation of realistic evasive maneuvers by the use of shaping filters," *Journal of Guidance, Control, and Dynamics*, vol. 2, no. 4, pp. 290–295, 1979.

[13] J. Shinar and D. Steinberg, "Analysis of optimal evasive maneuvers based on a linearized two-dimensional kinematic model," *Journal of Aircraft*, vol. 14, no. 8, pp. 795–802, 1977.

[15] R. J. Fitzgerald, "Shaping filters for disturbances with random starting times," *Journal of Guidance, Control, and Dynamics*, vol. 2, no. 2, pp. 152–154, 1979.

[16] A. Farina, B. Ristic, and D. Benvenuti, "Tracking a ballistic target: comparison of several nonlinear filters," *IEEE Trans. Aerosp. Electron. Syst.*, vol. 38, no. 3, pp. 854–867, 2002.

[17] R. Fonod and T. Shima, "Estimation Enhancement by Cooperatively Imposing Relative Intercept Angles," *Journal of Guidance, Control, and Dynamics*, vol. 40, no. 7, pp. 1711–1725, 2017.

[18] M. Rhudy, Y. Gu, and M. R. Napolitano, "An analytical approach for comparing linearization methods in EKF and UKF," *International Journal of Advanced Robotic Systems*, vol. 10, no. 4, p. 208, 2013.

[19] N. Shneydor, *Missile Guidance and Pursuit: Kinematics, Dynamics and Control*. Chichester, England: Horwood Publishing, 1998.

[20] V. Shaferman and T. Shima, "Cooperative multiple-model adaptive guidance for an aircraft defending missile," *Journal of Guidance, Control, and Dynamics*, vol. 33, no. 6, pp. 1801–1813, 2010.

[21] A. Ratnoo and T. Shima, "Line-of-sight interceptor guidance for defending an aircraft," *Journal of Guidance, Control, and Dynamics*, vol. 34, no. 2, pp. 522–532, 2011.

[22] S. Skogestad, "Simple analytic rules for model reduction and PID controller tuning," *Journal of Process Control*, vol. 13, no. 4, pp. 291–309, 2003.

[23] R. G. Cottrell, "Optimal intercept guidance for short-range tactical missiles," *AIAA journal*, vol. 9, no. 7, pp. 1414–1415, 1971.

[24] I.-S. Jeon, J.-I. Lee, and M.-J. Tahk, "Impact-time-control guidance law for anti-ship missiles," *IEEE Trans. Control Syst. Technol.*, vol. 14, no. 2, pp. 260–266, 2006.

[25] T. Shima, "Intercept-angle guidance," *Journal of Guidance, Control, and Dynamics*, vol. 34, no. 2, pp. 484–492, 2011.

[26] T. Shima, Y. Oshman, and J. Shinar, "Efficient multiple model adaptive estimation in ballistic missile interception scenarios," *Journal of Guidance, Control, and Dynamics*, vol. 25, no. 4, pp. 667–675, 2002.

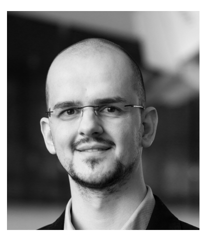

Robert Fonod (S'10–M'15) received the B.Sc. and M.Sc. degrees in cybernetics from the Technical University of Košice, Slovakia, in 2009 and 2011, respectively, and the Ph.D. degree in automatic control from the University of Bordeaux, France, in 2014.
He is currently an Assistant Professor with the Department of Space Engineering at the Delft University of Technology, the Netherlands. He was a Postdoctoral Research Fellow with the Department of Aerospace Engineering at the Technion–Israel Institute of Technology, Israel. His current research interests are in the area of guidance and estimation of aerospace vehicles, bearings-only target tracking, and model-based fault diagnosis.
Dr. Fonod is an Associated Editor for the IEEE TRANSACTIONS ON AEROSPACE AND ELECTRONIC SYSTEMS.

Tal Shima (SM'05) received the M.Sc. degree in aerospace engineering and the Ph.D. degree from the Technion–Israel Institute of Technology, Haifa, Israel, in 2001.
He is currently a Professor with the Department of Aerospace Engineering at the Technion. His current research interests include guidance of autonomous vehicles, especially missiles and aircraft, operating individually or as a team.
Prof. Shima is an Associate Fellow of AIAA and an Associate Editor for the IEEE TRANSACTIONS ON AEROSPACE AND ELECTRONIC SYSTEMS and IEEE TRANSACTIONS ON CONTROL SYSTEMS TECHNOLOGY.